

Inference skipping for more efficient real-time speech enhancement with parallel RNNs

Xiaohuai Le, Tong Lei, Kai Chen and Jing Lu

Abstract—Deep neural network (DNN) based speech enhancement models have attracted extensive attention due to their promising performance. However, it is difficult to deploy a powerful DNN in real-time applications because of its high computational cost. Typical compression methods such as pruning and quantization do not make good use of the data characteristics. In this paper, we introduce the Skip-RNN strategy into speech enhancement models with parallel RNNs. The states of the RNNs update intermittently without interrupting the update of the output mask, which leads to significant reduction of computational load without evident audio artifacts. To better leverage the difference between the voice and the noise, we further regularize the skipping strategy with voice activity detection (VAD) guidance, saving more computational load. Experiments on a high-performance speech enhancement model, dual-path convolutional recurrent network (DPCRN), show the superiority of our strategy over strategies like network pruning or directly training a smaller model. We also validate the generalization of the proposed strategy on two other competitive speech enhancement models.

Index Terms—speech enhancement, Dual-path RNN, Skip-RNN, model compression.

I. INTRODUCTION

SPEECH enhancement (SE) aims at separating clean speech from background interferences for higher speech intelligibility and perceptual quality. Conventional rule-based signal processing algorithms such as OMLSA [1] and MMSE-STSA [2] are widely used in real-time applications due to their small computational cost, but their performance deteriorates significantly in environments with non-stationary noise. In the last decade, data-driven SE algorithms based on deep neural network (DNN) have achieved remarkable progress with more noise suppression and higher speech quality than the conventional methods. Typical neural networks such as convolutional neural networks (CNNs) [3], recurrent neural networks (RNNs) [4] and more recently the attention mechanisms [5] have been successfully introduced to time-frequency domain [6], [7] and time domain [8], [9] SE. Generally, RNNs are suitable for real-time processing and attention is

more powerful in obtaining contextual information. Compared to other networks, CNNs require fewer parameters through weight sharing mechanism. With a convolutional encoder-decoder (CED) structure and the recurrent bottleneck, the recently proposed convolution recurrent network (CRN) [10] can take advantage of both CNNs and RNNs and has become popular in real-time SE [11], [12].

Most powerful DNNs that achieve promising SE performance require billions of floating-point operations per second. For low latency applications with limited computational resources, we need lightweight DNNs. In addition to designing a small neural network directly [13], compressing a large neural network by quantization [14] and pruning [15] is also feasible and has been used in SE recently [16]. Quantization reduces the bit width of weights and operators for faster inference while pruning removes the less important weights for less resource usage. Knowledge distillation method [17] trains a small network under the supervision of a larger network, and this has also been used in SE [18]. All these methods are applied at training stage and cannot be utilized to dynamically decrease the computational load according to the characteristics of input data during inference.

Skip-RNN [19] dynamically skips the state updates of RNN, which can theoretically reduce the computational load in inference. Some attempts of applying Skip-RNN have been made in SE [20]. One notable drawback of this strategy is that the output mask stops updating when the RNN skips, which results in audio artifacts. The exponential smoothing of hidden states [20] cannot effectively alleviate the problem. To fully solve this problem, it is necessary to skip the updates without interrupting the updates of mask by leveraging more reasonable network structures. On the other hand, the noisy speech features are often distributed unevenly across time and frequency domain. The noisy signal in practical applications may have the continuous pure noise frames, and they can be exploited to further reduce the computational cost without significant performance degradation.

We find that the interruption of the mask updates can be effectively circumvented in a network with parallel RNNs when applying the Skip-RNN strategy. Parallel RNNs have been used in various high performance SE models such as the convolutional U-net for speech enhancement (CRUSE) [12], [21], the gated convolutional recurrent network (GCRN) [11] and the dual-path convolutional recurrent network (DPCRN) [22]. In this paper, we take DPCRN as an example to discuss the application of Skip-RNN, which can be easily extended to CRUSE and GCRN. DPCRN combines the dual-path RNN (DPRNN) [23], a time domain speech separation network,

Manuscript received —, 2022; revised —, 2022; accepted —, 2022. Date of publication —, 2022; date of current version —, 2022. This work was supported by the National Natural Science Foundation of China under Grant 11874219. The associate editor coordinating the review of this manuscript and approving it for publication was —. (Corresponding author: —.)

Xiaohuai Le, Tong Lei, Kai Chen and Jing Lu are with the Key Laboratory of Modern Acoustics, Institute of Acoustics, Nanjing University, Nanjing 210093, China, with the NJU-Horizon Intelligent Audio Lab, Horizon Robotics, Beijing 100094, China, and also with the Nanjing Institute of Advanced Artificial Intelligence, Nanjing 210014, China (e-mail: xiaohuaile@smail.nju.edu.cn; tonglei@smail.nju.edu.cn; chenkai@nju.edu.cn; lujing@nju.edu.cn).

Digital Object Identifier 10.1109/TASLP.2019.2915167

and CRN in an effective way. Ranked at the 3rd place in Deep Noise Suppression-3 (DNS-3) challenge [24], it has much fewer parameters and lower computational burden than the other top models (0.8 M parameters and 3.7 G MACs, compared with 6.4 M parameters and 6.0 G MACs of Rank-1 model and 5.2 M parameters and 52.5 G MACs¹ of Rank-2 model), which makes it a very competitive real-time SE method. A huge number of parallel RNNs used in DPCRNN contribute significantly to the whole computational load, so it is meaningful to investigate efficient inference skipping strategies. In this paper, we apply Skip-RNN into DPRNN to reduce the computational load during inference. A binary gate is introduced in Skip-RNN to intermittently update the hidden states of RNNs. Due to the utilization of parallel RNNs, the mask will keep updating even when the hidden states stop updating. We investigate several regularization strategies to induce more skipped states while keeping a high quality enhanced speech. The CED structure used in DPCRNN can also mitigate audio artifacts. Furthermore, we observe a strong correlation between the skipping and the characteristics of noisy speech spectrogram. In pure noise frames, the states skip mechanism works more frequently. Inspired by this, we introduce a skipping control factor into Skip-RNN and integrate a VAD-guided skipping control method into our model, which can effectively save more computational load.

We test the efficacy of our proposed model by comparing its performance with that of the original DPCRNN through extensive experiments. To better illustrate the efficacy of the proposed model, we also compare it with another two models with the same computational load, i.e., a smaller model and the model compressed using network pruning technique. The results of multiple objective metrics show that with the same amount of computation the proposed method achieves significantly better performance. Experiments on other real-time SE models such as CRUSE and GCRN also show that our proposed strategy can significantly reduce the computational load while maintaining competitive performance.

II. MODEL DESCRIPTION

A. Problem Formulation

With the short time Fourier transform (STFT), the noisy speech can be expressed in the T-F domain as

$$X(t, f) = S(t, f) + N(t, f) \quad (1)$$

where $X(t, f)$, $S(t, f)$ and $N(t, f)$ represent the complex spectra of the noisy speech, the clean speech and the noise, respectively, with time index t and frequency index f . In order to recover clean speech from the mixture in the time-frequency domain, a common way is to estimate a mask and multiply it by the noisy speech $X(t, f)$ [7]. For phase retrieval, the complex ratio mask (CRM) is a widely used training target [25] which is denoted as a complex value $M_c(t, f)$. In [22], we used CRM to recover the phase implicitly and the denoising

process can be expressed as the complex product of the mask and the noisy speech as

$$\tilde{S}(t, f) = X(t, f) \odot M_c(t, f) \quad (2)$$

where \odot denotes element-wise multiplication and $\tilde{S}(t, f)$ is the enhanced speech. Compared with estimating magnitude mask only, CRM is more difficult to learn [11]. In this paper, we separately estimate masks for magnitude and phase spectrogram. Similar to PHASESEN [26], the model has three outputs, i.e. the magnitude mask $M(t, f)$ and the real and imaginary parts of the phase mask $\Phi(t, f)$. Finally, the noisy speech can be enhanced by

$$\tilde{S}(t, f) = X(t, f) \odot M(t, f) \odot \Phi(t, f). \quad (3)$$

Instead of estimating the masks directly, we apply the signal approximation (SA) [27] to optimize the target masks end-to-end. SA minimizes the difference between the enhanced speech and clean speech with the loss function described as $\mathcal{L} = Loss(\tilde{S}(t, f), S(t, f))$, where $Loss$ is the complex compressed spectrum MSE loss [12] in this paper.

B. Model Architecture

1) *Dual-Path Convolution Recurrent Network*: DPCRNN mainly consists of an encoder, a DPRNN [23] module and a decoder, as shown in Fig. 1. The model has three inputs X_r , X_i and X_p , which respectively denote the real part, the imaginary part of the noisy spectrogram and the logarithmic power spectrogram. They are concatenated as three channels of the input which can be denoted as a 3-D tensor $\mathbf{X} \in \mathbb{R}^{T \times F \times C}$, where T , F and $C = 3$ represent the dimensions of frequency, time and channel, respectively. The tensor normalized by batch normalization [28] is fed into the encoder to compress the frequency dimension to F_{en} and expand the channel dimension to C_{en} . The encoder uses the 2-D convolutional (Conv-2D) layers to extract the local patterns from the noisy spectrogram and get the output feature $\mathbf{X}_{en} \in \mathbb{R}^{T \times F_{en} \times C_{en}}$. In the DPRNN module, the feature is further processed by the intra-frame RNN block and the inter-frame RNN block (also known as the intra-chunk and the inter-chunk RNN block), as depicted in Fig. 2. The intra-frame RNNs are applied to the f -dimension of \mathbf{X}_{en} to model the spectral patterns in a single frame. As for the inter-frame RNNs, parallel RNNs are used to model the time dependence of the F_{en} sub-features.

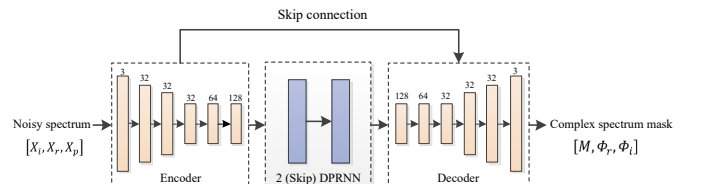


Fig. 1. The architecture of DPCRNN, including the encoder, the DPRNN module and the decoder. The numbers of channels for the convolutional layers are presented.

¹The computational complexity was not provided in the Rank-2 paper, so we implemented the model and calculated the MACs.

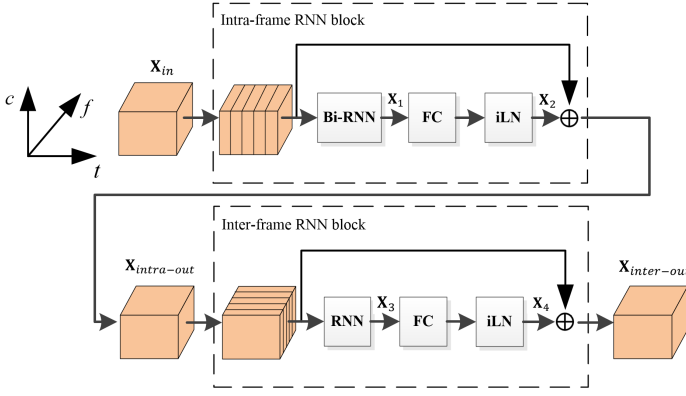


Fig. 2. The diagram of the DPRNN module. It consists of the intra-frame RNN block and the inter-frame RNN block.

For the input $\mathbf{X}_{in} \in \mathbb{R}^{T \times F_{in} \times C_{in}}$ of a DPRNN block (shown as the orange cube in Fig. 2), the output of the intra-frame RNN can be expressed as

$$\mathbf{X}_1 = [f_{RNN_{intra}}(\mathbf{X}_{in}[t, :, :]), t = 1, \dots, T] \quad (4)$$

where $\mathbf{X}_{in}[t, :, :] \in \mathbb{R}^{F_{in} \times C_{in}}$ is the sub-feature at time index t and $f_{RNN_{intra}}(\cdot)$ represents the function of the intra-frame RNN in the form of a bi-directional RNN with $C_{hid}/2$ channel output in each direction. The outputs of all frames are concatenated to form a 3-D tensor $\mathbf{X}_1 \in \mathbb{R}^{T \times F_{in} \times C_{hid}}$. A fully connected layer (FC) and the instant layer normalization (iLN) [29] are applied on \mathbf{X}_1 to transform the channel dimension back to C_{in} and normalize the feature respectively, expressed as

$$\mathbf{X}_2 = f_{LN_1}(f_{FC_1}(\mathbf{X}_1)) \quad (5)$$

where $f_{FC_1}(\cdot)$ and $f_{LN_1}(\cdot)$ respectively denote the functions of FC and iLN. To mitigate the gradient vanishing problem, a residual connection [30] is then applied between the input of intra-frame RNN and the output of iLN, expressed as

$$\mathbf{X}_{intra-out} = \mathbf{X}_2 + \mathbf{X}_{in} \quad (6)$$

where $\mathbf{X}_{intra-out} \in \mathbb{R}^{T \times F_{in} \times C_{in}}$ is the output of the intra-frame RNN block. Similarly, the inter-frame RNN processes the sub-features at different frequency indices, expressed as

$$\mathbf{X}_3 = [f_{RNN_{inter}}(\mathbf{X}_{intra-out}[:, f, :]), f = 1, \dots, F_{in}] \quad (7)$$

where $\mathbf{X}_{intra-out}[:, f, :] \in \mathbb{R}^{T \times C_{in}}$ is the sub-feature at frequency index f and $f_{RNN_{inter}}(\cdot)$ denotes the function of the inter-frame RNN. Similar to the sub-band SE method [31], the sub-features processed by the inter-frame RNN are mapped from certain sub-bands of the original spectrum. The unidirectional RNNs are used to model the time dependence of these sub-features in parallel to guarantee the causality of the whole model. With the FC layer, iLN and the residual connection, the output of the inter-frame RNN block is denoted as $\mathbf{X}_{inter-out} \in \mathbb{R}^{T \times F_{in} \times C_{in}}$, given by

$$\mathbf{X}_4 = f_{LN_2}(f_{FC_2}(\mathbf{X}_3)) \quad (8)$$

$$\mathbf{X}_{inter-out} = \mathbf{X}_4 + \mathbf{X}_{intra-out}. \quad (9)$$

The decoder uses the transposed convolutional layers to restore the features from the DPRNN module to the original

TABLE I
THE NUMBER OF TRAINABLE PARAMETERS AND MACs OF EACH MODULE OF THE BASELINE MODEL.

Operator type	MACs (M)	Parameters (M)
Encoder	83.71	0.042
Intra-frame RNN block $\times 2$	360.6	0.180
Inter-frame RNN block $\times 2$	458.8	0.230
Decoder	212.0	0.077
All	1115.1	0.529

size, forming a symmetric structure with the encoder. There are skip connections between the encoder and the decoder to pass the detailed information and further mitigate the gradient vanishing problem. The output of the decoder also has three channels, the first one is the magnitude mask M and the remaining two are normalized to obtain the real part and imaginary part of phase mask Φ , which are utilized in Eq. (3) to enhance the speech.

In this paper we replace the LSTM in the original DPCRNN with GRU [32], which yields little performance loss but saves a quarter of the computational load [12]. We also reduce the kernel size of the convolutional layers from (2,5) and (2,3) to (1,5) and (1,3), which reduces the complexity without significant performance loss [11]. We use 5 2-D convolutional layers in the encoder and set the strides as $\{(2,1), (2,1), (2,1), (1,1), (1,1)\}$. Note that the strides in the last two convolutional layers are (1,1) for sufficient frequency resolution of the features fed into the DPRNN module, which we found is important for speech quality [22]. We use two DPRNN modules and the resulting baseline DPCRNN has 0.53 M trainable parameters.

The baseline model enhances the noisy speech sampled at 16 kHz with a 32-ms frame length and a 16-ms hop length, resulting in 1115 M multiply-accumulate operations per second (MACs) during inference. Table I presents the MACs and trainable parameters of each module in the baseline model, from which we can find that the DPRNN module contributes the most to the model complexity. Besides, the convolutional layers can be more easily compressed by the quantization [14] technique. Therefore, we focus on the compression of the DPRNN module in this paper.

2) *Skip-RNN*: We apply Skip-RNN [19] in the DPRNN module for saving the computational load during inference. The hidden state of the conventional RNN updates in the form as

$$\tilde{s}_t = S(s_{t-1}, x_t) \quad (10)$$

where $S(\cdot, \cdot)$ is the update function and x_t is the input at time index t . Skip-RNN introduces a state update probability \tilde{p}_t which is usually mapped to a binary gate $g_t \in \{0, 1\}$ by a round function. The binary gate determines whether the hidden state needs to be updated to \tilde{s}_t or kept the same as the previous step s_{t-1} .

$$g_t = \text{round}(\tilde{p}_t) \quad (11)$$

$$s_t = g_t \tilde{s}_t + (1 - g_t) s_{t-1} \quad (12)$$

The probability \tilde{p}_t is cumulated by $\Delta \tilde{p}_t$, which is calculated from the hidden state of the previous step through a FC layer, given by

$$\Delta \tilde{p}_t = \sigma(\mathbf{W}_p s_{t-1} + b_p) \quad (13)$$

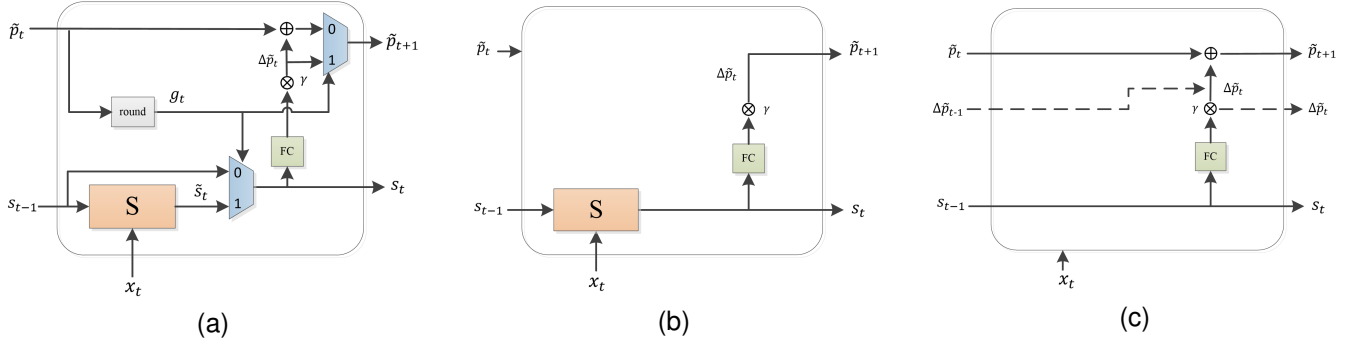


Fig. 3. The architecture of Skip-RNN with (a) the complete architecture at training, (b) the process of state updating and (c) the process of state skipping.

$$\tilde{p}_{t+1} = g_t \Delta \tilde{p}_t + (1 - g_t)(\tilde{p}_t + \min(\Delta \tilde{p}_t, 1 - \tilde{p}_t)) \quad (14)$$

where σ is the Sigmoid function to limit the output between 0 and 1. As shown in Eq. (14) and Fig. 3(a)(b), whenever a state update is skipped, the probability \tilde{p}_t is incremented by $\Delta \tilde{p}_t$ until \tilde{p}_t is high enough to update the state. As shown by the dashed lines in Fig. 3(c), $\Delta \tilde{p}_t$ only depends on the previous state and fixed when the state is fixed, so the update function Eq. (10) with the most computational load can be skipped when g_t is 0. The extra computational load of the additional layer shown in Eq. (13) is always negligible, so applying Skip-RNN can significantly reduce the computational load of the whole model. Moreover, for the structure like GRU, since the output is equal to the hidden state, the FC layers following the RNN can also be skipped when the state is fixed. We integrate Skip-RNN in the DPRNN module and get the Skip-intra-RNN and the Skip-inter-RNN respectively as

$$\mathbf{X}_1^t, \mathbf{g}_1^t = f_{Skip-RNN_{intra}}(\mathbf{X}_{in}[t, :, :]) \quad (15)$$

$$\mathbf{X}_3^f, \mathbf{g}_3^f = f_{Skip-RNN_{inter}}(\mathbf{X}_{intra-out}[:, f, :]) \quad (16)$$

$$\mathbf{X}_1 = [\mathbf{X}_1^t, t = 1, \dots, T] \quad (17)$$

$$\mathbf{X}_3 = [\mathbf{X}_3^f, f = 1, \dots, F_{in}] \quad (17)$$

$$\mathbf{g}_1 = [\mathbf{g}_1^t, t = 1, \dots, T] \quad (18)$$

$$\mathbf{g}_3 = [\mathbf{g}_3^f, f = 1, \dots, F_{in}] \quad (18)$$

where \mathbf{X}_1^t and \mathbf{X}_3^f are the outputs of the Skip-intra-RNN at time index t and the Skip-inter-RNN at frequency index f , respectively. Consistent with Eqs. (4) and (7), they are concatenated as the final output \mathbf{X}_1 and \mathbf{X}_3 . $\mathbf{g}_1^t \in \mathbb{R}^{1 \times F_{in}}$ and $\mathbf{g}_3^f \in \mathbb{R}^{T \times 1}$ respectively represent the binary gates of Skip-intra-RNN and Skip-inter-RNN and are also concatenated into $\mathbf{g}_1, \mathbf{g}_3 \in \mathbb{R}^{T \times F_{in}}$ which will be merged into the optimization targets during training. The computational complexity of Skip-RNN can be further measured by the update rate, which is defined as

$$update\ rate = \frac{1}{TF_{in}} \sum_t \sum_f \mathbf{g}[t, f] \quad (19)$$

The update rate calculates the percentage of the skipped states over a period of time.

We also propose a method to control the update rate of Skip-RNN to further regularize the computational load during

inference. The update of the hidden states of Skip-RNN depends on \tilde{p}_t which is cumulated by $\Delta \tilde{p}_t$. The increase rate of \tilde{p}_t can be easily adjusted by a scaling factor on $\Delta \tilde{p}_t$, expressed as

$$\Delta \tilde{p}_t = \gamma \sigma(\mathbf{W}_p s_{t-1} + b_p) \quad (20)$$

where γ is the scaling factor, so that the update rate can be controlled. When $\gamma < 1$, the hidden states update rate drops so that more computational load can be saved. This method can be easily implemented during inference without retraining.

To better exploit the characteristic of the signal spectrogram, we also integrate the voice activity detection (VAD) in our model under a multi-task learning framework. As shown in Fig. 4, the feature output from the encoder is processed by a 1×1 convolutional layer, after which the channel is compressed to 1. A GRU and a FC layer are then applied. The output of the FC layer is the probability of voice formed by the Sigmoid function. The dimension of the hidden states in the GRU is set to 32. The VAD estimator is optimized by minimizing the binary cross-entropy between the true labels and the predictions. Note that the VAD estimator is easy to be trained since we only require a high recall ratio of the voice frame. According to the estimated VAD labels, Eq. (20) will be utilized with different γ on the pure noise frames and the voice frames for further computational load adjustment.

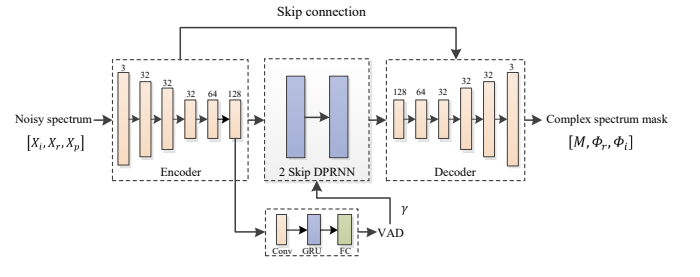


Fig. 4. The architecture of DPCRNN with the Skip-RNN and the VAD estimator.

C. Training Target

The complex compressed spectrum MSE loss [12] we use can be expressed as

$$\mathcal{L}_{SD} = \lambda MSE(S^c, \hat{S}^c) + (1 - \lambda) MSE(|S^c|^c, |\hat{S}^c|^c) \quad (21)$$

where $S = STFT(s)$ and $\hat{S} = STFT(\hat{s})$ denote the spectrogram of the clean speech s and the enhanced speech \hat{s} , and $MSE(\cdot)$ is the function of the mean squared error (MSE). Note that s and \hat{s} in a batch are normalized by the same factor for better optimization. In the first term of \mathcal{L}_{SD} , the spectrogram is compressed by

$$S^c = |S|^c \exp(j\theta_S) \quad (22)$$

where θ_S is the phase of S . In this paper, the spectrogram compression factor c and the loss weight factor λ are respectively set to 0.3 and 0.1 for higher speech quality [21].

We observe that directly training the model using Skip-RNN with loss function Eq. (21) cannot lead to a high skipping rate, so we use a regularization term to induce more skipped states in each Skip-RNN, expressed as

$$\mathcal{L}_{Skip} = \frac{1}{TF_{in}} \sum_i \left(\sum_t \sum_f \mathbf{g}_{1;i} [t, f] + \sum_t \sum_f \mathbf{g}_{3;i} [t, f] \right) \quad (23)$$

where $\mathbf{g}_{1;i}$ and $\mathbf{g}_{3;i}$ represent the binary gates of the Skip-intra-RNN and the Skip-inter-RNN in the i -th Skip-DPRNN module, respectively. The regularization term minimizes the sum of the mean values of the binary gates for higher compression rate. To obtain a specified compression rate, we can also optimize the states update rate of each Skip-RNN to the target rate by

$$\mathcal{L}_{Skip} = \sum_i \left(\left(\frac{1}{TF_{in}} \sum_t \sum_f \mathbf{g}_{1;i} [t, f] - \mu_{1;i} \right)^2 + \left(\frac{1}{TF_{in}} \sum_t \sum_f \mathbf{g}_{3;i} [t, f] - \mu_{3;i} \right)^2 \right) \quad (24)$$

where $\mu_{1;i}$ and $\mu_{3;i}$ are the target update rate of the Skip-intra-RNN and the Skip-inter-RNN in the i -th Skip-DPRNN module, respectively. In addition to MSE, the mean absolute error (MAE) can also be used as a regularization term, given by

$$\mathcal{L}_{Skip} = \sum_i \left(\left| \frac{1}{TF_{in}} \sum_t \sum_f \mathbf{g}_{1;i} [t, f] - \mu_{1;i} \right| + \left| \frac{1}{TF_{in}} \sum_t \sum_f \mathbf{g}_{3;i} [t, f] - \mu_{3;i} \right| \right) \quad (25)$$

Compare with MSE, MAE can accelerate the convergence. The final loss function can be expressed as a weighted sum of \mathcal{L}_{SD} and \mathcal{L}_{Skip} , given as

$$\mathcal{L} = \mathcal{L}_{SD} + \alpha \mathcal{L}_{Skip} \quad (26)$$

where α is a weighting factor.

III. EXPERIMENTS

A. Datasets

All the experiments are conducted on the WSJ0 SI-84 dataset [33]. We select 14633 utterances (about 25 h) from 120

speakers, including 12776 in training set, 1206 in validation set and 651 in test set. In order to improve the generalization on various noises, we also use the noise dataset from the DNS-3 Challenge [24]. The dataset also includes 60000 audio clips from DEMAND [34], Audioset [35] and Freesound² for a total of 150 hours.

To improve the robustness against the variation of the signal levels, the reverberation and the coloring effects of speech signal in practical applications, we use the data augmentation pipeline from [36] in training. Specifically, the clean speech is split into 11212 8-second segments, 30% of which will be filtered by a second-order IIR spectral augmentation filters. Consistent with [12], [13], all the filter coefficients are uniformly distributed in $[-3/8, 3/8]$. After spectral augmentation, half of the audio clips are convolved with room impulse responses (RIRs) randomly-selected from openSLR26 and openSLR28 [37]. Then the noisy speech is generated by mixing reverberant speech and noise. The signal-to-noise ratio (SNR) of the mixture is randomly sampled between -5 and 5 dB. Finally, the noisy and clean speech is scaled by the same factor drawn from a Gaussian distribution on the denary logarithmic scale with mean -0.5 and variance 1. The level scaling factor will also be used in Eq. (21) for normalization. The validation set is generated in the same way as the training set.

For the test set, we use two unseen noise datasets. One is the music data from MUSAN [38], the other includes the babble, factory1 and f16 noise from NOISEX92 [39]. The noises are mixed with the speech at SNR of -5, 0 and 5 dB, with 651 mixtures for each SNR level and each dataset. Considering the audio with long pure noise frames in practical applications, we also generate a test set of long noisy speech. We concatenate the test speech in pairs, and there are 8-second silent audio between every pair. We randomly mix the long speech and music noises at the SNR uniformly sampled between -5 to 5 dB. In total, we generate 3906 segments of short audio and 325 segments of long audio for test³.

B. Experiment Configuration

The window length and hop size used in our models are 32 ms and 16 ms respectively, resulting in a total latency of 48 ms. The FFT length is 512 and the frequency dimension F of the input is 257. The sine window is applied before FFT and overlap-add. The baseline model is called DPCRn-base, in which the hidden dimension C_{hid} of every GRU and Bi-GRU is 128. We reduce C_{hid} to control the computational complexity of DPCRn-base for comparison in two ways. One is by directly training a smaller model, named as DPCRn-S, and the other is by applying the structured pruning method described in [40], named as DPCRn-P, with the intrinsic sparse structures-based ℓ_2 -norm integrated in Eq. (21) as the loss function.

We apply Skip-RNN in the intra-frame RNNs and the inter-frame RNNs, and name the resulting models DPCRn-Intra-skip and DPCRn-Inter-skip respectively. In order to explore

²<https://freesound.org/>

³The source code of our proposed model can be found at <https://github.com/Le-Xiaohuai-speech/SKIP-DPCRn>

TABLE II
PERFORMANCE OF OUR PROPOSED MODELS ON TWO TEST SETS.

Test set		NOISEX				MUSAN			
Models	α	SDR (in dB)	PESQ	STOI (in %)	Update rate	SDR (in dB)	PESQ	STOI (in %)	Update rate
Noisy	-	0.091	1.433	74.94	-	0.043	2.004	80.76	-
DPCRN-base	-	9.527	2.688	89.13	1.00	11.54	3.105	93.69	1.00
Intra-skip	5×10^{-5}	9.508	2.681	88.87	0.712	11.53	3.084	93.55	0.679
Intra-skip	1×10^{-4}	9.448	2.670	88.86	0.482	11.48	3.076	93.54	0.456
Intra-skip	2×10^{-4}	9.394	2.672	88.76	0.436	11.37	3.065	93.41	0.419
Intra-skip	3×10^{-4}	9.358	2.649	88.49	0.271	11.24	3.042	93.17	0.258
Inter-skip	5×10^{-5}	9.409	2.666	88.67	0.765	11.45	3.068	93.38	0.709
Inter-skip	1×10^{-4}	9.424	2.662	88.63	0.640	11.39	3.059	93.30	0.545
Inter-skip	2×10^{-4}	9.355	2.633	88.24	0.426	11.26	3.031	93.01	0.393
Inter-skip	3×10^{-4}	9.355	2.640	88.30	0.359	11.27	3.024	93.02	0.328
All-skip	5×10^{-5}	9.405	2.654	88.57	0.745	11.42	3.056	93.29	0.706
All-skip	1×10^{-4}	9.337	2.645	88.53	0.577	11.29	3.014	93.20	0.524

the compression capacity of Skip-RNN, we also replace all the RNNs with Skip-RNNs and name the resulting model DPCRN-All-skip. The models are trained by minimizing Eq. (26) with one regularization term from Eqs. (23) and (24), as explicitly described in Sec. IV.

Based on DPCRN-All-skip, we further explore the multi-task learning framework with a VAD estimator. The ideal VAD labels are generated using energy thresholds of the clean speech. During inference, the output $\tilde{v}(t)$ of the estimator is smoothed by the rules expressed as

$$v(t) = \begin{cases} 0, & \text{if } \tilde{v}(t), \tilde{v}(t-1), \dots, \tilde{v}(t-9) = 0 \\ 1, & \text{otherwise.} \end{cases} \quad (27)$$

where $v(t)$ is the final VAD estimation of the t -th frame. The smoothing strategy improves the recall ratio of the voice frames at the expense of VAD accuracy.

All the models are trained by the Adam optimizer [41] with a batch size of 16. The initial learning rate is 1e-3 and it will be halved if the loss on the validation set does not improve for 10 consecutive epochs. Early stopping is also applied in training if the loss on the validation set does not improve for 20 epochs. For structured pruning, the loss function with the ℓ_2 -norm regularization is used first, then the weights of RNNs and corresponding FCs are pruned by their magnitude, after which the models are fine-tuned for 50 epochs with the original loss of Eq. (21). TensorFlow is employed for model implementation and a Nvidia TITAN Xp is used for training.

C. Models for Comparison and Evaluation Metrics

Apart from DPCRN, we also apply the proposed Skip-RNN strategy to two more real-time SE models, i.e., CRUSE [12], [21] and GCRN [11], to further validate its efficacy. CRUSE is a well-studied model which achieves a promising tradeoff between computational load and performance. GCRN uses a gating mechanism and group RNNs, achieving competitive performance in real-time SE. We build the CRUSE model in the same way as [21], which has 8 convolutional layers and a GRU bottleneck with 4 parallel subgroups. As for GCRN, we follow the same structure as [11], but replace LSTMs with

TABLE III
MACs, TRAINABLE PARAMETER NUMBERS OF PROPOSED MODELS AND THE AVERAGE UPDATE RATE OF EACH RNN BLOCK.

Models	α	Intra-RNN update rate	Inter-RNN update rate	MACs (M)	Para. (M)
DPCRN-base	-	1.00	1.00	1115	0.5286
Intra-skip	5×10^{-5}	0.696	1.00	1005	0.5288
Intra-skip	1×10^{-4}	0.469	1.00	923.6	0.5288
Intra-skip	2×10^{-4}	0.427	1.00	908.6	0.5288
Intra-skip	3×10^{-4}	0.265	1.00	849.7	0.5288
Inter-skip	5×10^{-5}	1.00	0.737	1011	0.5288
Inter-skip	1×10^{-4}	1.00	0.575	994.4	0.5288
Inter-skip	2×10^{-4}	1.00	0.410	844.2	0.5288
Inter-skip	3×10^{-4}	1.00	0.344	814.0	0.5288
All-skip	5×10^{-5}	0.702	0.749	892.5	0.5291
All-skip	1×10^{-4}	0.520	0.581	749.8	0.5291

GRUs. The number of parameters of these two models are 8.58 M and 7.66 M, respectively. The frame length and hop size in both models are 20 ms and 10 ms. We use the loss function Eq. (26) with the regularization Eq. (25) to train these models, because we find MAE leads to faster convergence than MSE when the hidden size of RNN is large.

We use three objective metrics for performance evaluation: the signal-to-distortion ratio (SDR) [42], the perceptual evaluation of speech quality (PESQ) [43], and the short-time objective intelligibility (STOI) [44].

IV. RESULTS AND DISCUSSIONS

A. The Efficacy of Skip-RNN

To demonstrate the efficacy of Skip-RNN, we compare the performance of DPCRN-base and the model with Skip-RNN. Table (II) presents the performance and the average states update rate on two test sets. All the models with Skip-RNN are trained by minimizing the loss function Eq. (26) with the regularization Eq. (23) weighted by α . Table (III) shows the average states update rate, the average MACs and the number of parameters of every model. Note that the average update

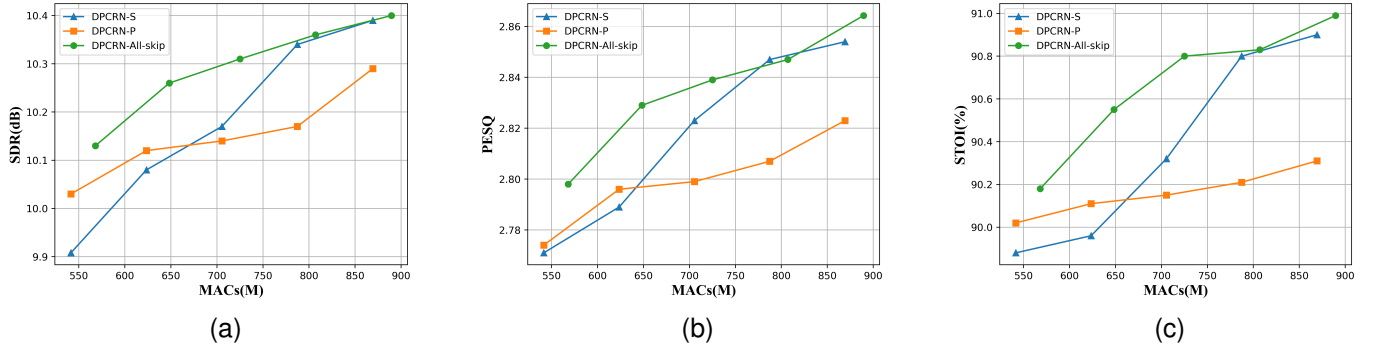


Fig. 5. The average performance of DPCRNN-All-skip with update rates of $\{0.3, 0.4, 0.5, 0.6, 0.7\}$ and DPCRNN-S and DPCRNN-P with compression rates of $\{0.3, 0.4, 0.5, 0.6, 0.7\}$.

rate of Skip-RNN slightly differs between different test sets, so we show the average update rate of all the test sets in Table II.

From Tables II and III, one can get the following conclusions. Firstly, integrating Skip-RNN saves significant computational load with limited performance degradation. Secondly, it can also be found that the performance is positively correlated with the amount of computation. Note that although DPCRNN-Intra-skip obtains lower update rate than DPCRNN-Inter-skip with the same α , its overall computational load shown in Table III is higher because the amount of computation of an intra-frame RNN is a quarter fewer than an inter-frame RNN. Therefore, DPCRNN-Intra-skip gets higher objective metric scores than DPCRNN-Inter-skip with the same α . Thirdly, as α increases, the regularization term leads to more frequent skipping and lower update rate, which can be considered as a form of dynamic temporal pruning. The states update rate relates to both the regularization factor α and the noise characteristics during inference. Specifically, the performance on the MUSAN test set is superior to the NOISEX test set in terms of all the metrics but the update rate is lower, demonstrating that the model will update more frequently under more disruptive noises and “slack off” under more tractable noises. This makes it possible to further reduce the computational load. Lastly, although DPCRNN-All-skip has overall inferior performance, it exceeds two DPCRNN-Inter-skip models with fewer MACs when $\alpha = 1 \times 10^{-4}$, which indicates applying Skip-RNN on all RNNs with a proper α can achieve a good balance between performance and computation. In addition to the results of the average computational load, the distributions of the frame level update rates of the DPRNN module in DPCRNN-All-skip ($\alpha = 1 \times 10^{-4}$) are shown in Fig. 6. The frame-level computational load is distributed like a Gaussian distribution and the peak computational load is reduced by about 15%.

B. Compression Rate Comparison

To further illustrate the compression performance of the Skip-RNN strategy, Eq. (26) with Eq. (24) are used as the loss ($\alpha = 1 \times 10^{-2}$) to train the DPCRNN-All-skip models with the target update rate respectively set to $\{0.3, 0.4, 0.5, 0.6, 0.7\}$. For comparison, we obtain DPCRNN-S by directly

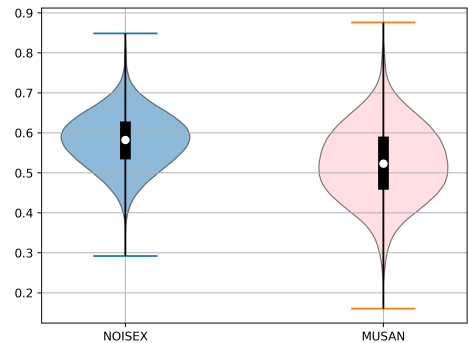


Fig. 6. The distributions of the frame level update rates of the DPRNN module in DPCRNN-All-skip ($\alpha = 1 \times 10^{-4}$).

training a smaller model and DPCRNN-P using structured pruning. The hidden dimensions of the intra-frame and the inter-frame RNNs of both models are reduced to $\{(48,52), (60,65), (74,77), (86,89), (96,100)\}$, leading to the compression rates of $\{0.3, 0.4, 0.5, 0.6, 0.7\}$, so that all the models can be compared with similar computational load. The results of the three methods are shown in Fig. 5. The average computational load shown by the green line is always higher than expectation, indicating that the achieved update rates of DPCRNN-All-skip on the test sets are always a little higher than the target update rates set in training. Even so, it still can be seen that DPCRNN-All-skip outperforms the other two models in most cases. When the compression rate is greater than about 0.6, the performance of DPCRNN-S is comparable with that of DPCRNN-All-skip. DPCRNN-P performs worst at a higher compression rate, but with decreasing compression rate, it gradually exceeds DPCRNN-S. A possible reason is that the regularization term of the pruning method brings significant weights sparsity, which makes it difficult to fine-tune the model at a higher compression rate.

C. More Efficient Inference by VAD-guided Skipping

Fig. 7 shows the spectrogram processed by DPCRNN-All-Skip ($\alpha = 1 \times 10^{-4}$) on a noisy sample with two utterances

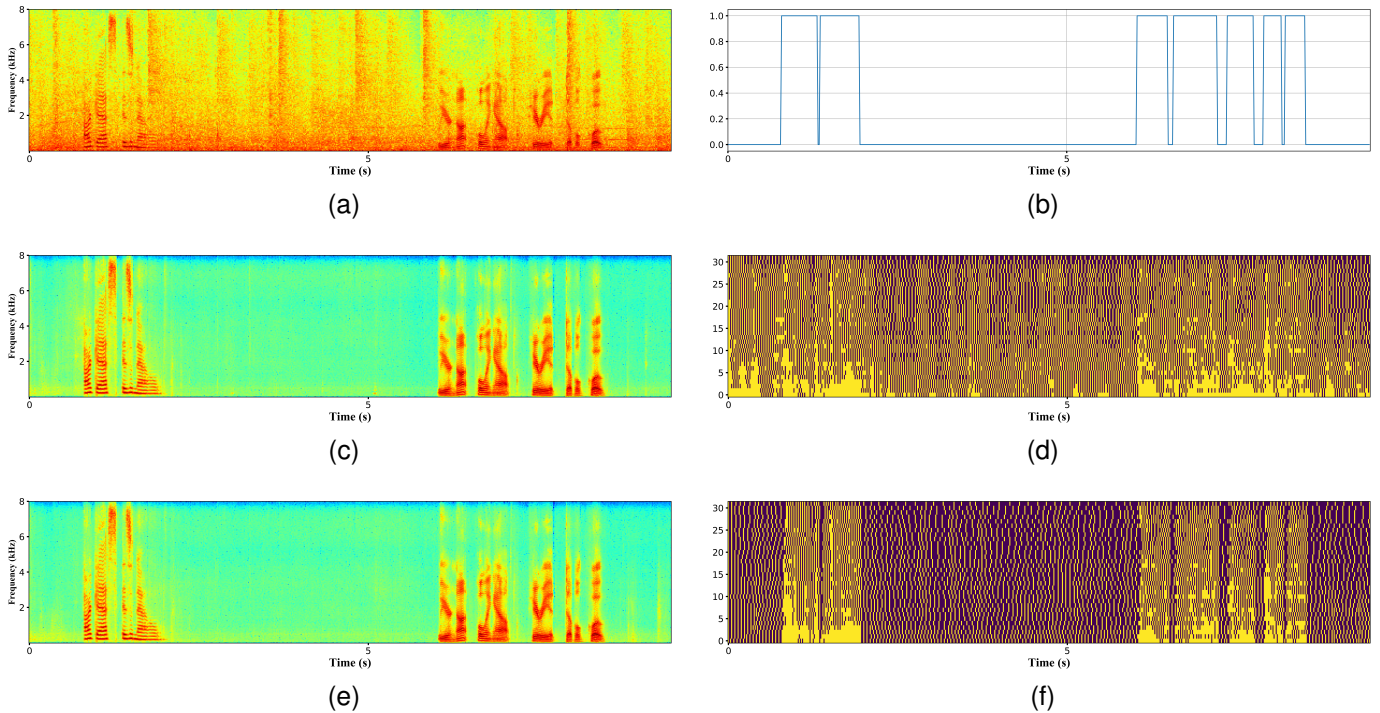


Fig. 7. Spectrogram visualization and binary gate visualization of the last Skip-inter-RNN. (a) Noisy speech. (b) The VAD labels of the clean speech. (c) Enhanced speech by DPCR-All-skip. (d) The binary gate visualization of the last Skip-inter-RNN. (e) Enhanced speech by DPCR-All-skip with the VAD-guided skipping strategy. (f) The binary gate visualization of the last Skip-inter-RNN with the VAD-guided skipping strategy.

and long pure noise segments. The binary gate $g_{3;2}$ of the last Skip-inter-RNN is also visualized as a 2-D map in Fig. 7(d), where the horizontal and the vertical axes respectively denote time and the index of parallel RNNs. The bright bins in the map represent the updated states of RNNs and the dark bins represent the skipped states. From the map and the noisy spectrogram, we can observe the similarity between the distribution of the bright bins and the spectral envelope of the noisy speech. At noise segments, the hidden states are skipped significantly more frequently than the voice segments, which illustrates why the model “slacks off” at more tractable scenarios. Inspired by this, we can reduce the update rate at pure noise frames to further save the computational load while hold the original update rate at voice frames. Guided by the ideal VAD label shown in Fig. 7(b), the probability rescaling factor γ is set to 0.4 at pure noise frames and 1 at voice frames. Then we use Eq.(20) to control the update rate. The results shown in Fig. 7(e)(f) illustrate that the Skip-RNNs skip more frequently at pure noise segments without spectrogram artifacts.

We test the VAD-guided skipping strategy on the long audio test set. DPCR-All-skip is trained with a VAD estimator and the target average update rate is set to 0.5. We apply different γ only at pure noise frames and the objective results are shown in Fig. 8(a)(b)(c). As expected, the performance deteriorates significantly when γ is less than 0.3. However, all the metrics with the ideal VAD labels do not show a monotonic increasing trend, and the model even achieves the same SDR score as DPCR-base (shown as the green dotted lines) when $\gamma = 0.4$,

because pure noise frames can be more effectively attenuated⁴. Using the estimated VAD labels leads to weaker performance than using the ideal labels, but the SDR and PESQ curves still show the benefit of small γ . Overall, the model gets the best results when $\gamma = 0.5$ and the computational load of the DPRNN modules at pure noise segments is only 28% of the baseline. Fig. 8(d) presents the average update rates with different γ . The average update rates are almost constant at voice frames and demonstrate a close to linear relationship with γ at pure noise frames, which allows the model to preserve speech while further reduce the computational load. The accuracy of the VAD estimator on the long audio test set is 88.2%. Note that the VAD estimator is not the focus of this paper and in practice better estimators may lead to higher performance.

D. Results on CRUSE and GCRN

Table IV presents the results of CRUSE and GCRN, where CRUSE-base and GCRN-base are the baseline models using the conventional RNN, and CRUSE-skip and GCRN-skip use Skip-RNN. It can be seen that after applying Skip-RNN, the two models remain the comparable performance to the baseline models with a significantly lower update rate, which indicates that Skip-RNN can be fused into any model that use parallel RNN structure. The final update rates of GCRN-skip is higher than CRUSE-skip because the former utilizes fewer parallel RNNs with a higher hidden dimension, which makes

⁴Exemplary audio samples can be found at <https://github.com/Le-Xiaohuai-speech/SKIP-DPCR-samples>

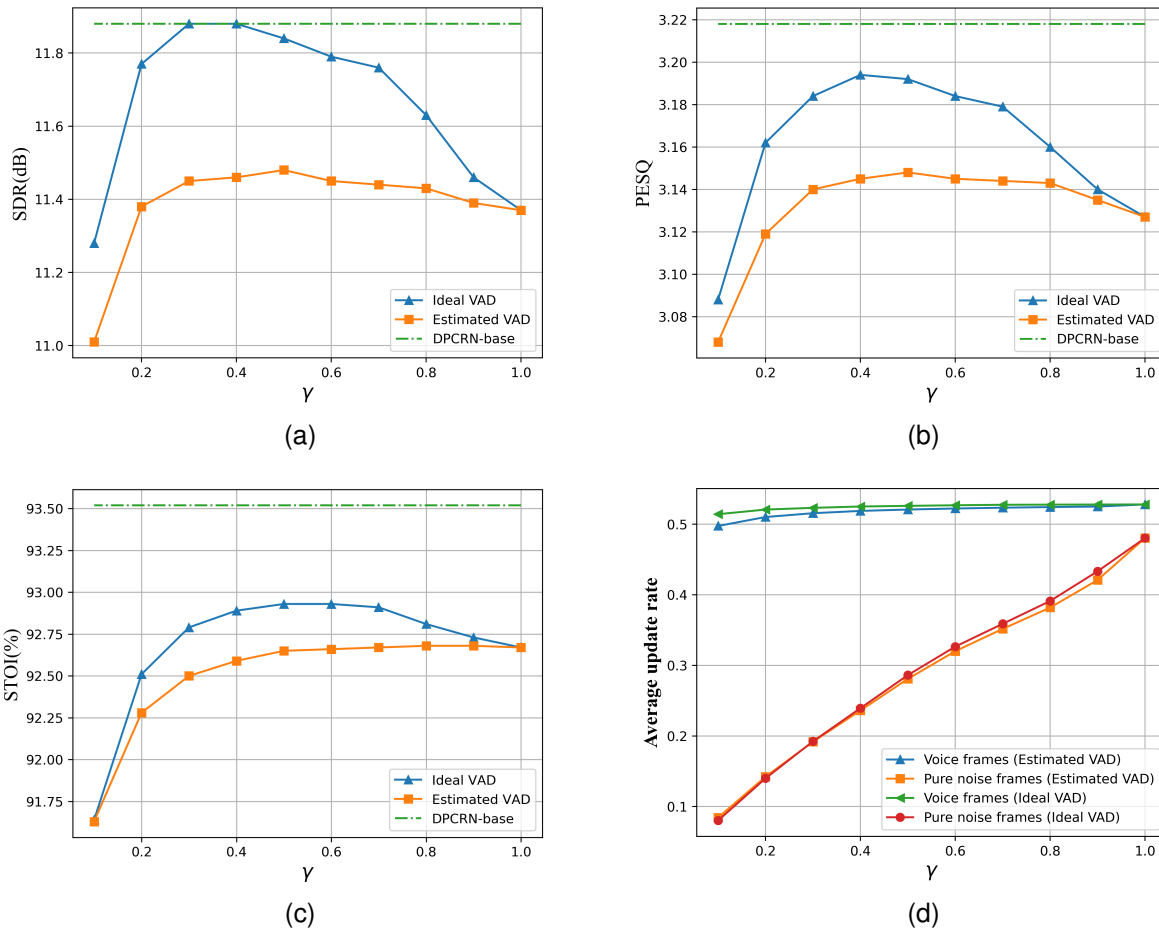


Fig. 8. Results of the VAD-guided skipping strategy on the long audio test set. (a) SDR scores, (b) PESQ scores and (c) STOI scores at different γ . (d) The average update rates on voice and pure noise frames at different γ .

TABLE IV
PERFORMANCE OF CRUSE AND GCRN ON TWO TEST SETS SETS.

Test set Metrics	NOISEX				MUSAN			
	SDR (in dB)	PESQ	STOI (in %)	Update rate	SDR (in dB)	PESQ	STOI (in %)	Update rate
Noisy	0.091	1.433	74.94	-	0.043	2.004	80.76	-
CRUSE-base	8.423	2.457	85.65	1.00	10.29	2.834	91.41	1.00
CRUSE-skip	8.426	2.457	85.58	0.496	10.25	2.822	91.27	0.491
GCRN-base	9.393	2.359	87.32	1.00	11.19	2.654	91.58	1.00
GCRN-skip	9.348	2.364	87.07	0.697	11.14	2.650	91.36	0.642

the model harder to optimize. In addition, the audio artifacts described in [20] are not observed in all experiments, which is mainly due to the parallel RNNs and the CED structure. The parallel RNNs reduce the impact of the skipping on the updates of the output and the detailed information transferred from the encoder by the CED structure helps further recover the speech.

V. CONCLUSION

Parallel RNNs have been proven to be an important module for several high performance speech enhancement models. In this paper, we find that it is effective to introduce the Skip-RNN strategy into these models since the RNNs can

be updated intermittently without interrupting the update of the output mask. Therefore the computational burden can be significantly reduced without evident audio artifacts. Using DPCRN as an example, we investigate several regularization strategies to induce more skipped states and introduces a VAD estimator to better exploit the characteristics of the noisy spectrogram. The experimental results demonstrate the superiority of the proposed model over those from the commonly used compression strategies, i.e., directly training a smaller model and structured pruning. Experiments on CRUSE and GCRN also validate the generalization of the proposed inference skipping strategy.

REFERENCES

- [1] I. Cohen and B. Berdugo, "Speech enhancement for non-stationary noise environments," *Signal Process.*, vol. 81, no. 11, pp. 2403–2418, 2001.
- [2] M. Kato, A. Sugiyama, and M. Serizawa, "Noise suppression with high speech quality based on weighted noise estimation and mmse stsa," *IEICE Trans. Fundamentals*, vol. 85, no. 7, pp. 1710–1718, 2002.
- [3] A. Li, W. Liu, C. Zheng, C. Fan, and X. Li, "Two heads are better than one: A two-stage complex spectral mapping approach for monaural speech enhancement," *IEEE/ACM Trans. Audio, Speech, Lang. Process.*, vol. 29, pp. 1829–1843, 2021.
- [4] L. Sun, J. Du, L.-R. Dai, and C.-H. Lee, "Multiple-target deep learning for lstm-rnn based speech enhancement," *IEEE Hands-free Speech Communications and Microphone Arrays (HSCMA)*, pp. 136–140, 2017.
- [5] J. Kim, M. El-Khamy, and J. Lee, "T-gsa: Transformer with gaussian-weighted self-attention for speech enhancement," in *Proc. IEEE Int. Conf. Acoust., Speech, Signal Process.*, 2020, pp. 6649–6653.
- [6] Y. Xu, J. Du, L.-R. Dai, and C.-H. Lee, "A regression approach to speech enhancement based on deep neural networks," *IEEE/ACM Trans. Audio, Speech, Lang. Process.*, vol. 23, no. 1, pp. 7–19, 2015.
- [7] D. Wang and J. Chen, "Supervised speech separation based on deep learning: An overview," *IEEE/ACM Trans. Audio, Speech, Lang. Process.*, vol. 26, no. 10, pp. 1702–1726, 2018.
- [8] S. Pascual, A. Bonafonte, and J. Serra, "SEGAN: Speech Enhancement Generative Adversarial Network," in *Proc. Interspeech*, 2017, pp. 3642–3646.
- [9] S.-W. Fu, T.-W. Wang, Y. Tsao, X. Lu, and H. Kawai, "End-to-end waveform utterance enhancement for direct evaluation metrics optimization by fully convolutional neural networks," *IEEE/ACM Trans. Audio, Speech, Lang. Process.*, vol. 26, no. 9, pp. 1570–1584, 2018.
- [10] H. Zhao, S. Zarar, I. Tashev, and C.-H. Lee, "Convolutional-recurrent neural networks for speech enhancement," in *Proc. IEEE Int. Conf. Acoust., Speech, Signal Process.*, 2018, pp. 2401–2405.
- [11] K. Tan and D. Wang, "Learning complex spectral mapping with gated convolutional recurrent networks for monaural speech enhancement," *IEEE/ACM Trans. Audio, Speech, Lang. Process.*, vol. 28, pp. 380–390, 2020.
- [12] S. Braun, H. Gamper, C. K. Reddy, and I. Tashev, "Towards efficient models for real-time deep noise suppression," in *Proc. IEEE Int. Conf. Acoust., Speech, Signal Process.*, 2021, pp. 656–660.
- [13] J.-M. Valin, "A hybrid dsp/deep learning approach to real-time full-band speech enhancement," in *Proc. IEEE 20th Int. Workshop Multimedia Signal Process. (MMSp)*, 2018, pp. 1–5.
- [14] B. Jacob, S. Kligys, B. Chen, M. Zhu, M. Tang, A. Howard, H. Adam, and D. Kalenichenko, "Quantization and training of neural networks for efficient integer-arithmetic-only inference," in *Proc. IEEE Conf. Comput. Vis. Pattern Recognit.*, 2018, pp. 2704–2713.
- [15] P. Molchanov, S. Tyree, T. Karras, T. Aila, and J. Kautz, "Pruning convolutional neural networks for resource efficient inference," in *Proc. Int. Conf. Learn. Represent.*, 2017. [Online]. Available: <https://arxiv.org/pdf/1611.06440>
- [16] K. Tan and D. Wang, "Towards model compression for deep learning based speech enhancement," *IEEE/ACM Trans. Audio, Speech, Lang. Process.*, vol. 29, pp. 1785–1794, 2021.
- [17] G. Hinton, O. Vinyals, and J. Dean, "Distilling the knowledge in a neural network," *Comput. Sci.*, vol. 14, no. 7, pp. 38–39, 2015.
- [18] X. Hao, S. Wen, X. Su, Y. Liu, G. Gao, and X. Li, "Sub-Band Knowledge Distillation Framework for Speech Enhancement," in *Proc. Interspeech*, 2020, pp. 2687–2691.
- [19] V. Campos, B. Jou, X. Giro-i-Nieto, J. Torres, and S.-F. Chang, "Skip rnn: Learning to skip state updates in recurrent neural networks," in *Proc. Int. Conf. Learn. Represent.*, 2017. [Online]. Available: <https://ui.adsabs.harvard.edu/abs/2017arXiv170806834C>
- [20] I. Fedorov, M. Stamenovic, C. Jensen, L.-C. Yang, A. Mandell, Y. Gan, M. Mattina, and P. N. Whatmough, "TinyLSTMs: Efficient Neural Speech Enhancement for Hearing Aids," in *Proc. Interspeech*, 2020, pp. 4054–4058.
- [21] S. Braun and H. Gamper, "Effect of noise suppression losses on speech distortion and ASR performance," *arXiv e-prints*, p. arXiv:2111.11606, Nov. 2021.
- [22] X. Le, H. Chen, K. Chen, and J. Lu, "DPCRN: Dual-Path Convolution Recurrent Network for Single Channel Speech Enhancement," in *Proc. Interspeech*, 2021, pp. 2811–2815.
- [23] Y. Luo, Z. Chen, and T. Yoshioka, "Dual-path rnn: Efficient long sequence modeling for time-domain single-channel speech separation," in *Proc. IEEE Int. Conf. Acoust., Speech, Signal Process.*, 2020, pp. 46–50.
- [24] C. K. Reddy, H. Dubey, K. Koishida, A. Nair, V. Gopal, R. Cutler, S. Braun, H. Gamper, R. Aichner, and S. Srinivasan, "INTERSPEECH 2021 Deep Noise Suppression Challenge," in *Proc. Interspeech*, 2021, pp. 2796–2800.
- [25] D. S. Williamson, Y. Wang, and D. Wang, "Complex ratio masking for monaural speech separation," *IEEE/ACM Trans. Audio, Speech, Lang. Process.*, vol. 24, no. 3, pp. 483–492, 2016.
- [26] D. Yin, C. Luo, Z. Xiong, and W. Zeng, "Phasen: A phase-and-harmonics-aware speech enhancement network," in *Proc. Assoc. Advancement Artificial Intelligence (AAAI)*, vol. 34, no. 05, 2020, pp. 9458–9465.
- [27] F. Weninger, J. R. Hershey, J. Le Roux, and B. Schuller, "Discriminatively trained recurrent neural networks for single-channel speech separation," in *Proc. IEEE Global Conf., Signal Inf. Process.*, 2014, pp. 577–581.
- [28] K. He, X. Zhang, S. Ren, and J. Sun, "Delving deep into rectifiers: Surpassing human-level performance on imagenet classification," in *Proc. IEEE Int. Conf. Comput. Vis.*, 2015, pp. 1026–1034.
- [29] J. L. Ba, J. R. Kiros, and G. E. Hinton, "Layer normalization," *stat*, vol. 1050, pp. 21–34, 2016.
- [30] K. He, X. Zhang, S. Ren, and J. Sun, "Deep residual learning for image recognition," in *Proc. IEEE Conf. Comput. Vis. Pattern Recognit.*, 2016, pp. 770–778.
- [31] X. Hao, X. Su, R. Horaud, and X. Li, "Fullsubnet: A full-band and sub-band fusion model for real-time single-channel speech enhancement," in *Proc. IEEE Int. Conf. Acoust., Speech, Signal Process.*, 2021, pp. 6633–6637.
- [32] K. Cho, B. van Merriënboer, D. Bahdanau, and Y. Bengio, "On the properties of neural machine translation: Encoder–decoder approaches," in *Proc. 8th Workshop Syntax, Semantics Structure Statistical Translation*, 2014, pp. 103–111.
- [33] D. B. Paul and J. M. Baker, "The design for the wall street journal-based csr corpus," in *Proc. Workshop Speech Natural Lang.*, 1992, pp. 357–362.
- [34] J. Thiemann, N. Ito, and E. Vincent, "The diverse environments multi-channel acoustic noise database (demand): A database of multichannel environmental noise recordings," *J. Acoustical Soc. Amer.*, vol. 133, p. 3591, 2013.
- [35] J. F. Gemmeke, D. P. W. Ellis, D. Freedman, A. Jansen, W. Lawrence, R. C. Moore, M. Plakal, and M. Ritter, "Audio set: An ontology and human-labeled dataset for audio events," in *Proc. IEEE Int. Conf. Acoust., Speech, Signal Process.*, 2017, pp. 776–780.
- [36] S. Braun and I. Tashev, "Data augmentation and loss normalization for deep noise suppression," in *Proc. Speech Comput.* Springer, 2020, pp. 79–86.
- [37] T. Ko, V. Peddinti, D. Povey, M. L. Seltzer, and S. Khudanpur, "A study on data augmentation of reverberant speech for robust speech recognition," in *Proc. IEEE Int. Conf. Acoust., Speech, Signal Process.*, 2017, pp. 5220–5224.
- [38] D. Snyder, G. Chen, and D. Povey, "Musan: A music, speech, and noise corpus," *arXiv preprint arXiv:1510.08484*, 2015.
- [39] A. Varga and H. Steeneken, "Assessment for automatic speech recognition: Ii. noisex-92: A database and an experiment to study the effect of additive noise on speech recognition systems," *Speech Commun.*, vol. 12, pp. 247–251, 1993.
- [40] W. Wen, Y. He, S. Rajbhandari, M. Zhang, W. Wang, F. Liu, B. Hu, Y. Chen, and H. Li, "Learning

- intrinsic sparse structures within long short-term memory,” in *Proc. Int. Conf. Lear. Represent.*, September 2017. [Online]. Available: <https://www.microsoft.com/en-us/research/publication/learning-intrinsic-sparse-structures-within-long-short-term-memory/>
- [41] D. P. Kingma and J. Ba, “Adam: A Method for Stochastic Optimization,” in *Proc. Int. Conf. Lear. Represent.*, 2014. [Online]. Available: <https://arxiv.org/abs/1412.6980>
- [42] E. Vincent, R. Gribonval, and C. Fevotte, “Performance measurement in blind audio source separation,” *IEEE Trans. Signal Process.*, vol. 14, no. 4, pp. 1462–1469, 2006.
- [43] A. W. Rix, J. G. Beerends, M. P. Hollier, and A. P. Hekstra, “Perceptual evaluation of speech quality (pesq)-a new method for speech quality assessment of telephone networks and codecs,” in *Proc. IEEE Int. Conf. Acoust., Speech, Signal Process.*, vol. 2, 2001, pp. 749–752 vol.2.
- [44] C. Taal, R. Hendriks, R. Heusdens, and J. Jensen, “A short-time objective intelligibility measure for time-frequency weighted noisy speech,” in *Proc. IEEE Int. Conf. Acoust., Speech, Signal Process.*, 2010, pp. 4214 – 4217.